Solid-State Electronics 208 (2023) 108738

Contents lists available at ScienceDirect

Solid State Electronics

journal homepage: www.elsevier.com/locate/sse

A multi-level cell for ultra-scaled STT-MRAM realized by back-hopping ☆

M. Bendra [a,b,*], S. Fiorentini [a,b], S. Selberherr [b], W. Goes [c], V. Sverdlov [a,b]

[a] Christian Doppler Laboratory for Nonvolatile Magnetoresistive Memory and Logic, Gußhausstraße 27–29, Wien, A-1040, Austria
[b] Institute for Microelectronics, TU Wien, Gußhausstraße 27–29, Wien, A-1040, Austria
[c] Silvaco Europe Ltd., Compass Point, St Ives, Cambridge, PE27 5JL, United Kingdom

ARTICLE INFO

Keywords:
Back-hopping
Spin transfer torques
Ultra-scaled MRAM cells
Perpendicular magnetic anisotropy
Writing error
Multi-level cells

ABSTRACT

The development of advanced magnetic tunnel junctions with a footprint in the single-digit nanometer range can be achieved using structures with an elongated and composite ferromagnetic free layer. Using the spin drift-diffusion model, we investigated the back-hopping effect in ultra-scaled STT-MRAM devices. Unwanted switching of the last layer of the structure has been identified as a possible cause of the back-hopping effect, which leads to a writing error in the magnetization state of the free layer. To understand the switching of the free layer, the torque acting on both parts of the composite free layer must be studied in detail. A reduction in the size of MRAM components to increase the memory density may lead to back-hopping. Moreover, the observed back-hopping effect can be exploited for the realization of multi-level cells. For this purpose, we have carefully investigated the switching behavior of a device with several tunnel barrier interfaces and a few nanometers in diameter, in particular the impact of changes in the material parameters.

1. Introduction

Spin-transfer torque magnetoresistive random access memory (STT-MRAM) is one of the most promising candidates for nonvolatile memory technologies. In particular, STT-MRAM technology is attractive for Computing-in-Memory concepts [1], embedded automotive systems [2], low-latency industrial applications [3], last-level cache for microprocessors [4], and high-density MRAM arrays [5]. These diverse applications highlight the potential of STT-MRAM technology in different fields and its versatility in meeting various requirements.

An STT-MRAM cell consists of several layers, including a CoFeB reference layer (RL) and a free magnetic layer (FL) separated by an MgO tunnel barrier (TB), which form a magnetic tunnel junction (MTJ). To increase the perpendicular magnetic anisotropy, the FL, typically composed of two CoFeB layers and a thin metal buffer, is interfaced with a second MgO layer [6]. Elongating the FL and introducing additional MgO layers allows to even further increase the perpendicular anisotropy, while also reducing the cell diameter [7].

However, if the length of the FL falls below a certain threshold or at higher current densities [8], we predict an undesired switching of the FL section, which gives rise to the back-hopping effect. This effect leads to a writing error in the magnetization state of the free layer, which could be detrimental to the reliability of the memory. Nonetheless, this effect can subsequently be exploited to realize multi-level cells (MLC) by properly adjusting the polarization of the TB.

To further enhance memory density, a MLC based on more than one MTJ is proposed [9]. However, the implementation of a MLC requires careful tuning of the characteristics of each MTJ, leading to the formation of multiple stable states [10]. Therefore, there is a need to understand the magnetization dynamics of magnetic materials related to the performance of MTJs in order to accurately design a MLC.

2. Micromagnetics model

We developed a modeling and simulation approach based on a fully three-dimensional finite element method which accurately describes the transport of charge and spin in nanometer-sized MTJs [11]. Our approach includes all relevant physical phenomena responsible for the proper functioning of ultra-scaled MRAM cells.

To extend the method to MTJs, we model the TB as a poor conductor with a local conductivity which depends on the relative orientation of the magnetization. We supplement the model with appropriate boundary conditions for the spin current $\mathbf{J}_S^{TB}$ at the TB interfaces to account for the dependence of the torque on the relative magnetization orientation specific to MTJs [12]:

$$\mathbf{J}_C^{TB} = J_0(V)(1 + P_{RL}P_{FL} \cdot \cos\theta) \quad (1)$$

☆ The review of this paper was arranged by Sorin Cristoloveanu.

* Corresponding author at: Christian Doppler Laboratory for Nonvolatile Magnetoresistive Memory and Logic, Gußhausstraße 27–29, Wien, A-1040, Austria.
E-mail address: bendra@iue.tuwien.ac.at (M. Bendra).

https://doi.org/10.1016/j.sse.2023.108738

Available online 7 August 2023

Table 1
Simulation parameters.

Parameter	Value
Gilbert damping, α	0.015
Gyromagnetic ratio, γ	$1.76 \cdot 10^{11}\ \frac{\text{rad}}{\text{s T}}$
Saturation magnetization, M_S	1.51 T
Exchange constant, A	$1 \cdot 10^{-11}\ \frac{\text{J}}{\text{m}}$
Free layer length, t_{FL}	X nm
Interface anisotropy, K_i	1.53 mT
Uniaxial anisotropy constant, K	K_i/t_{FL}
Current spin polarization, β_σ	0.7
Diffusion spin polarization, β_D	1.0
Electron diffusion coefficient, D_e	$2 \cdot 10^{-2}\ \frac{\text{m}^2}{\text{s}}$
Spin-flip length, λ_{sf}	10 nm
Exchange length, λ_J	1 nm
Spin dephasing length, λ_φ	0.4 nm
Electrical resistance in the anti-parallel state, R_{AP}	750 kΩ
Electrical resistance in the parallel state, R_P	410 kΩ

$$\mathbf{J_S^{TB}} = -\frac{\mu_B}{e}\frac{\mathbf{J_C^{TB}}\cdot\mathbf{n}}{1+P_{RL}P_{FL}\mathbf{m_{RL}}\cdot\mathbf{m_{FL}}}\cdot \cdot[P_{RL}\mathbf{m_{RL}} + P_{FL}\mathbf{m_{FL}} + {}^1\!/_2(P_{RL}^{\eta}P_{RL} - P_{FL}^{\eta}P_{FL})\mathbf{m_{RL}}\times\mathbf{m_{FL}}] \quad (2)$$

Eq. (1), portrays the correlation of the charge current density at the interface, denoted as $\mathbf{J_C^{TB}}$, with the RL and FL polarization parameters and the angle between their respective magnetization vectors. It represents the charge current density at the interface as being directly proportional to a voltage-dependent portion of the current density $J_0(V)$. This product is further influenced by the cosine of the angle between the magnetizations of RL and FL and their respective in-plane Slonczewski polarization parameters P_{RL} and P_{FL}. The boundary condition, denoted as Eq. (2), is essential for properly evaluating the spin current and the spin accumulation in the RL and the FL, respectively. $\mathbf{n}$ is the interface normal, $\mathbf{m_{RL(FL)}}$ is the magnetization of the RL and FL, $P_{RL(FL)}$ are in-plane Slonczewski polarization parameters, P_{RL}^{η} and P_{FL}^{η} are out-of-plane polarization parameters, μ_B is the Bohr magneton, and e is the elementary charge.

By using (2), we describe the spin and charge transport coupled to the magnetization in arbitrary stacks of MTJs and metallic spin valves with a unified drift-diffusion approach. This approach provides a proper analysis of the sequential switching of a FL consisting of two ferromagnetic pieces FL_1 and FL_2 separated by a tunnel junction. Overall, our approach can provide an accurate and comprehensive understanding of the transport of spin and charge in MTJs, which can aid in the development of advanced MRAM technology.

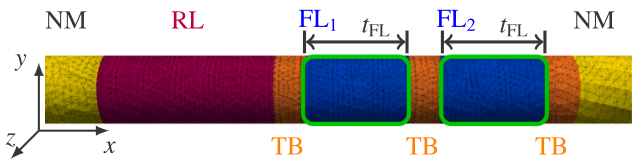

Fig. 1. A simplified mesh representation of an ultra-scaled MRAM cell. This composite structure consists of a CoFeB (5)|MgO (0.9)|CoFeB (5)|MgO (0.9)|CoFeB (5)|MgO (0.9) MTJ connected to normal metal contacts (50), where the numbers in parentheses indicate the length of each layer in nanometers. The diameter is 2.3 nm. A bias of 1.5 V is applied across the structure. The color coding is as follows: purple for the RL, blue for the FL, orange for the TB, and yellow for the non-magnetic contacts (NM). The green framed section denotes the FL segments for FL_1 and FL_2, with the length t_{FL}.

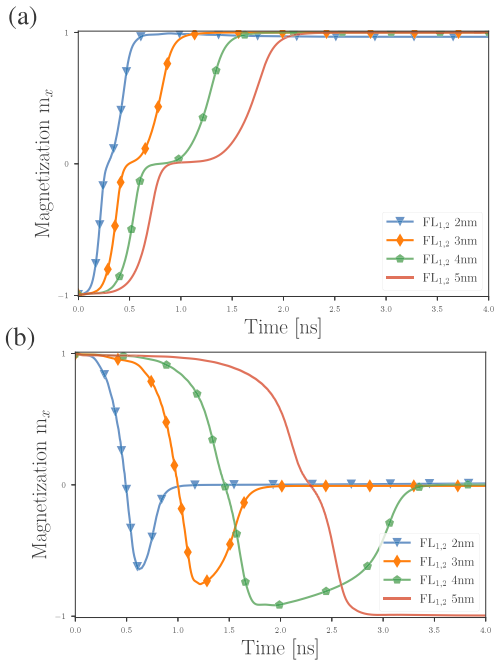

Fig. 2. Magnetization trajectories for the switching from (a) AP to P and (b) P to AP for different combinations of FL lengths. The polarization of the TB is 0.6, 0.5, and 0.2, in order from left to right in Fig. 1.

3. Results

The following sections report the results of switching simulations performed in the structure depicted in Fig. 1. The parameters employed are presented in Table 1 [7,13].

In Fig. 2 the magnetization trajectories for the switching from anti-parallel (AP) to parallel (P) and from P to AP of an ultra-scaled MRAM with symmetric FL configurations are displayed. The applied bias is 1.5 V or −1.5 V depending on the magnetization switching direction, P to AP, or AP to P. Fig. 2(a) reports, that the successful switching of the FL from AP to P is always obtained. Fig. 2(b) shows that successful switching from P to AP is only obtained for a larger length t_{FL} of 5 nm.

The differences in the response times of the cells are due to the different uniaxial anisotropies which depend on the length of the layer. A shorter layer possesses a reduced energy barrier separating the two magnetization configurations, so that the speed of the response is improved in the case of the shorter layer.

In Fig. 3 we report switching realizations where we modeled the polarization of the TBs, such that the TB in the middle of the FL is the higher one. In Fig. 3(a), all structures switch successfully except for a FL length of 2 nm. Here, the magnetization develops a single oscillation before reaching a stable state. This oscillation is due to the weak anisotropy, and the torques from FL_2 acting on FL_1 being more substantial than from RL, leading to an initial back-and-forth switching before reaching the final state. In the AP configuration, the pre-established direction for the voltage flow is negative, which corresponds to the traditional 'positive' direction in terms of electron flow. Thus, the electrons move in the opposite direction to the defined voltage flow. In this AP setup the RL exerts a torque on FL_1, driving it in the positive x-direction to align it parallel with the RL. At the same time FL_2 exerts a torque on FL_1 in the same direction, establishing an antiparallel orientation with respect to FL_2. The cumulative effect of these torques precipitates the initial switching of FL_1. As this happens,

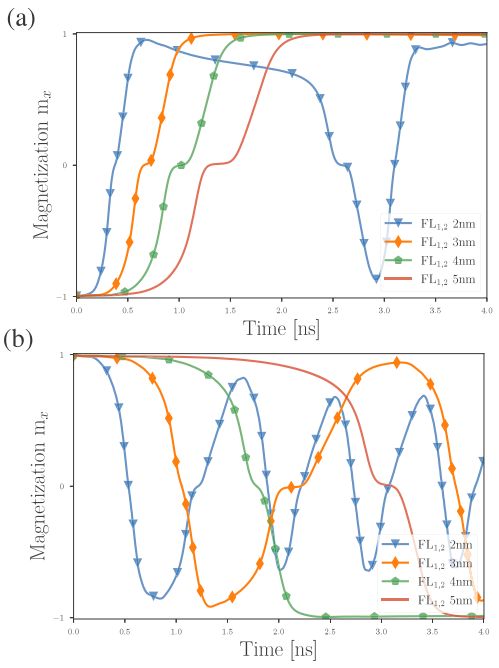

Fig. 3. Magnetization trajectories for the switching from (a) AP to P and (b) P to AP for different combinations of FL lengths, were we applied the same methodology as in Fig. 1, but with increasing polarization of TB in the middle of the FL. The polarization of the TB is 0.5, 0.9, and 0.2, in order from left to right in Fig. 1. In addition, the symmetrical structure with 3 nm thick FLs has the best prerequisites for a MLC.

the torque applied from FL_1 towards FL_2 promotes parallel alignment of the two magnetization vectors, maintaining FL_2 in its original state. However, upon the switch of FL_1's magnetization, the torque imposed on FL_2 undergoes a sign change, compelling it to switch subsequently too.

Fig. 3(b) illustrates the back-hopping effect. The structure with 3 nm length shows continuous transitions between the sequence of states as long as the bias is applied. The sequential switching procedure of the composite FL is as follows: During the switching from the P to AP configuration, the process evolves in an opposite manner. The torque from FL_2 acting on FL_1 opposes that from the RL. On the other hand, the torque from FL_1 acting on FL_2 supports magnetization inversion, prompting FL_2 to switch initially. After FL_2's switch, the torques from both FL_2 and the RL act on FL_1 in the same direction, finalizing the switching process.

As the bias is maintained, the magnetization of FL_2 reverses due to the higher polarization in the middle TB and the back-hopping effect of FL_2 occurs. The torques from the RL favor the anti-parallel state and those from FL_2 favor the parallel state. However, due to the higher polarization in the middle TB, the torques from FL_2 are stronger than those from the RL, so FL_1 flips, and the whole FL returns to the initial configuration. This process repeats as long as the bias is maintained.

A higher polarization refers to the degree to which the electrons passing through the tunnel barrier are polarized in terms of their spin orientation. A higher TB polarization means that a larger fraction of electrons are spin-polarized, which in turn results in a higher spin current passing through the barrier. The spin current is responsible for the transfer of angular momentum from the electrons to the magnetic moment of the FL, resulting in a torque which causes the magnetization to switch direction.

Therefore, when the TB polarization is higher, a stronger spin current is generated, which causes a stronger torque to act on the FL segments (FL_1 and FL_2) than on the RL and FL_1, as shown in Fig. 4. This means that when the middle TB polarization is the highest, the back-hopping of the FL segments occurs more easily.

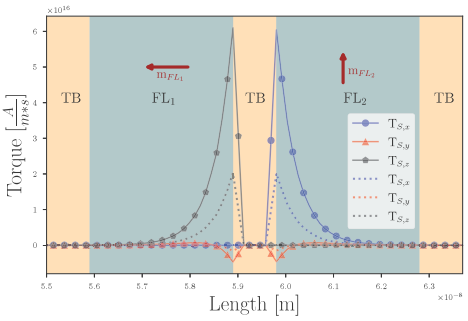

Fig. 4. The torque computed with the spin-current boundary condition (2) for an MTJ with semi-infinite ferromagnetic layers. The magnetization is along x in the RL and the FL_1, and along z in the FL_2. The three curves represent x-, y-, and z-components of the computed spin torque, along an axis going through the center of the structure. Brown vectors report the magnetization direction in both ferromagnetic layers. Dotted lines represent the polarization of the TB used in Fig. 2 and the solid line with markers represents the polarization used in Fig. 3.

In Fig. 5 we report switching realizations with different duration of the applied bias. By adjusting the duration of the bias pulse, we can realize a multi-level cell with four distinctly different states. These states of the FL are illustrated by the blue arrows and they follow the same switching procedure as mentioned earlier. By properly modulating the duration of the pulse, all four states can be addressed. A distinction between the two intermediate states can be recognized by the fact that the first state FL_1 parallel to the RL and anti-parallel to FL_2 has a lower resistance than the state with FL_1 anti-parallel to the RL and FL_2.

4. Conclusion

The coupled spin and charge drift-diffusion approach is supplemented with appropriate boundary conditions for the spin current $\mathbf{J_S}$ at the TB interfaces to account for the dependence of the torque on the relative magnetization orientation specific to MTJs. This boundary condition is key to describe the spin current and the spin accumulations in the RL and FL. This gives the opportunity to describe the spin and charge transport coupled to the magnetization in arbitrary stacks of MTJs. We demonstrated an appearance of the back-hopping effect in ultra-scaled STT-MRAM devices with a composite free layer. By proper analysis of the back-hopping effect, we demonstrated the potential of employing this effect to engineer devices as a multi-bit cells with four different states.

Declaration of competing interest

The authors declare that they have no known competing financial interests or personal relationships that could have appeared to influence the work reported in this paper.

Data availability

Data will be made available on request.

Acknowledgments

The financial support by the Federal Ministry of Labour and Economy, the National Foundation for Research, Technology and Development, the Christian Doppler Research Association, and the TU Wien Bibliothek for financial support through its Open Access Funding Program is gratefully acknowledged.

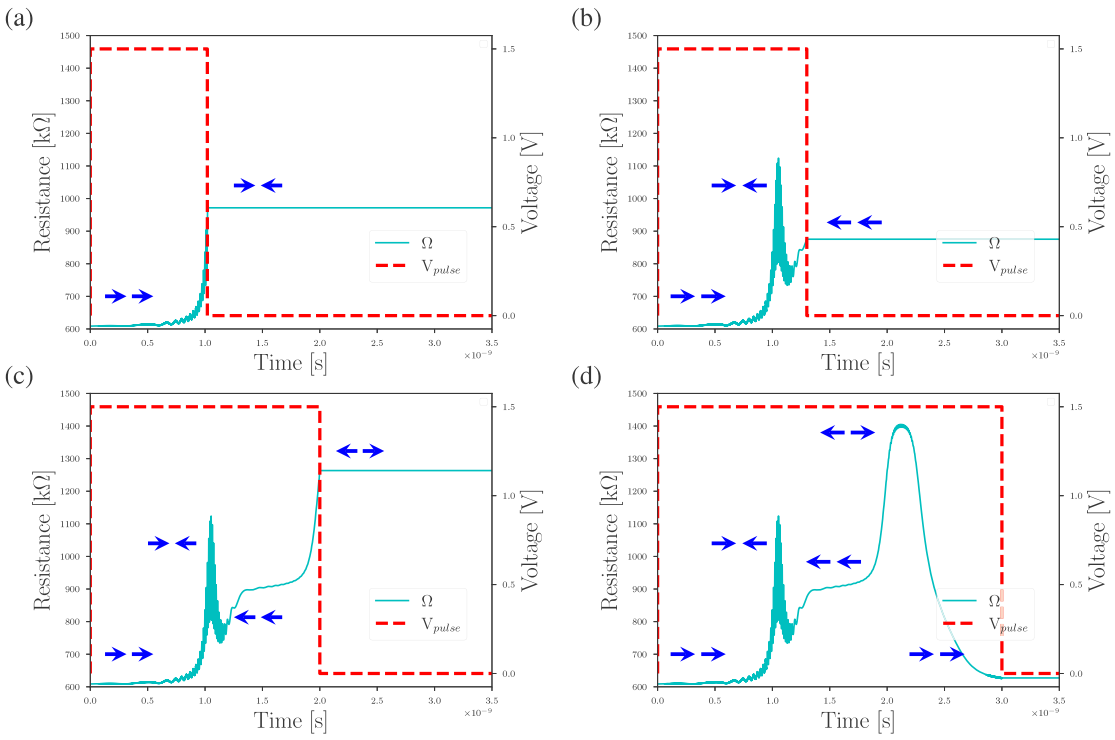

Fig. 5. Resistance trajectories for a symmetric structure with 3 nm thick FLs, switching from P to AP for different duration of the applied bias. The solid blue line represents the resistance of the cell during the switching process and the red dashed line the duration and amplitude of the bias pulse. The arrows along the trajectories represent the state of FL_1 and FL_2.

References

[1] Jung S, Lee H, Myung S, Kim H, Yoon SK, Kwon S-W, Ju Y, Kim M, Yi W, Han S, et al. A crossbar array of magnetoresistive memory devices for in-memory computing. Nature 2022;601:211–6. http://dx.doi.org/10.1038/s41586-021-04196-6.

[2] Naik VB, Yamane K, Lee T, Kwon J, Chao R, et al. JEDEC-qualified highly reliable 22nm FD-SOI embedded MRAM for low-power industrial-grade, and extended performance towards automotive-grade-1 applications. In: IEEE International electron devices meeting. IEDM, 2020, p. 11.3.1–4. http://dx.doi.org/10.1109/IEDM13553.2020.9371935.

[3] Ikegawa S, Nagel K, Mancoff FB, Alam SM, Arora M, DeHerrera M, Lee HK, Mukherjee S, Shimon G, Sun JJ, Rahman I, Neumeyer F, Chou HY, Tan C, Shah A, Aggarwal S. High-speed (400MB/s) and low-BER STT-MRAM technology for industrial applications. In: IEEE International electron devices meeting. IEDM, 2022, p. 10.4.1–4. http://dx.doi.org/10.1109/IEDM45625.2022.10019513.

[4] Hu G, Safranski C, Sun JZ, Hashemi P, Brown SL, Bruley J, Buzi L, D'Emic CP, Galligan E, Gottwald MG, Gunawan O, Lee J, Karimeddiny S, Trouilloud PL, Worledge DC. Double spin-torque magnetic tunnel junction devices for last-level cache applications. In: IEEE International electron devices meeting. IEDM, 2022, p. 10.2.1–4. http://dx.doi.org/10.1109/IEDM45625.2022.10019402.

[5] Seo SM, Aikawa H, Kim SG, Nagase T, Ito Y, Ha TJ, Yoshino K, Jung BK, Oikawa T, Jung KY, Moon HI, Kim BS, Matsuoka F, Hatsuda K, Hoya K, Kim S, Lee S-H, Na M-H, Cha SY. First demonstration of full integration and characterization of $4f^2$ 1S1M cells with 45 nm of pitch and 20 nm of MTJ size. In: IEEE International electron devices meeting. IEDM, 2022, p. 10.1.1–4. http://dx.doi.org/10.1109/IEDM45625.2022.10019549.

[6] Sato H, Yamanouchi M, Ikeda S, Fukami S, Matsukura F, Ohno H. MgO/CoFeB/Ta/CoFeB/MgO recording structure in magnetic tunnel junctions with perpendicular easy axis. IEEE Trans Magn (TMAG) 2013;49:4437–40. http://dx.doi.org/10.1109/TMAG.2013.2251326.

[7] Jinnai B, Igarashi J, Watanabe K, Funatsu T, Sato H, et al. High-performance shape-anisotropy magnetic tunnel junctions down to 2.3 nm. In: IEEE International electron devices meeting. IEDM, 2020, p. 24.6.1–4. http://dx.doi.org/10.1109/IEDM13553.2020.9371972.

[8] Abert C, Ruggeri M, Bruckner F, Vogler C, Manchon A, et al. A self-consistent spin-diffusion model for micromagnetics. Sci Rep 2016;6. http://dx.doi.org/10.1038/s41598-016-0019-y.

[9] Chiu Y-C, Yang C-S, Teng S-H, Huang H-Y, Chang F-C, et al. A 22nm 4Mb STT-MRAM data-encrypted near-memory computation macro with a 192GB/s read-and-decryption bandwidth and 25.1-55.1TOPS/W 8b MAC for AI operations. In: IEEE International solid- state circuits conference (ISSCC), Vol. 65. 2022, p. 178–80. http://dx.doi.org/10.1109/ISSCC42614.2022.9731621.

[10] Cai W, Wang M, Cao K, Yang H, Peng S, et al. Stateful implication logic based on perpendicular magnetic tunnel junctions. Sci China Inf Sci 2022;65. http://dx.doi.org/10.1007/s11432-020-3189-x.

[11] Fiorentini S, Jørstad NP, Ender J, de Orio RL, Selberherr S, Bendra M, Goes W, Sverdlov V. Finite element approach for the simulation of modern MRAM devices. Micromachines 2023;14. http://dx.doi.org/10.3390/mi14050898.

[12] Fiorentini S, Bendra M, Ender J, de Orio RL, Goes W, Selberherr S, Sverdlov V. Spin and charge drift-diffusion in ultra-scaled MRAM cells. Sci Rep 2022;12. http://dx.doi.org/10.1038/s41598-022-25586-4.

[13] Ikeda S, Miura K, Yamamoto H, Mizunuma K, Gan HD, et al. A perpendicular-anisotropy CoFeB–MgO magnetic tunnel junction. Nat Mater 2010;9:721–4. http://dx.doi.org/10.1038/nmat2804.